ADVANCED FUNCTIONAL MATERIALS
www.afm-journal.de

Upcycling Spent Cathode Materials to Bifunctional Catalysts for High-Stability Lithium–Sulfur Batteries

Hengyao Zhu, Shiming Chen, Xiangming Yao, Kai Yang, Wenguang Zhao, Taowen Chen, Luyi Yang, and Feng Pan**

In order to enhance the sluggish kinetics and suppress the polysulfide shuttle effect in high-loading lithium–sulfur (Li–S) batteries, it is crucial to design and synthesize catalysts exhibiting both high conversion rate and strong anchoring effect toward polysulfide species. Herein, based on theoretical predictions, spent cathode materials ($LiCoO_2$ and $LiMn_2O_4$) from spent lithium-ion batteries are converted into a bifunctional catalyst (Co—MnO) for Li–S batteries through the high-temperature shock method. Owing to the synergistic catalytic and anchoring effect of polysulfide species exhibit by Co—MnO, superior electrochemical performance, including excellent rate performance (707 mAh g^{-1} at 4C) and high stability (capacity fading of 0.058% per cycle over 400 cycles at 1C) can be delivered under a low areal catalyst loading (<0.5 wt%). This work not only offers a new design strategy for Li–S catalysts, but also proposes a promising approach to transform spent LIBs into highly efficient catalysts.

1. Introduction

The rapid development of energy storage devices has led to the development of next-generation batteries with high energy density, capabilities of quick charging and discharging, and considerable lifespan.[1,2] Lithium–sulfur (Li–S) batteries, launched by a chain of stepwise conversion redox reactions, have stood out from other electrochemical power sources due to the low costs, high specific capacity, and environmental sustainability.[3–5] Nevertheless, the slow reaction kinetics, large volume swings, and the shuttle effect of lithium polysulfides (LiPSs)[6–8] are the main technological hurdles for the commercialization of Li–S batteries. Compared with other approaches, such as separator coatings,[9] electrolyte regulation,[10] and anode modification,[11] loading catalysts on the cathode side is considered the most direct and effective one as it could be imposed on sulfur cathodes, regulating both the confining and conversion of LiPSs.

On the one hand, the unique electron orbital configuration and arrangement of catalysts introduce adsorption sites to achieve chemical adsorption of polysulfides.[7,12] For instance, different researchers introduced silicon oxide,[13] porous carbon,[14] or metal alloy[15] into cathodes. All the doped materials, respectively, not only result in plenty of spaces confining LiPSs, but also provide additional impetus to polysulfide adsorption through chemical interaction. On the other hand, the surficial structure of catalysts could promote the conversion kinetics of LiPSs by lowering the activation energy and enhance the utilization of sulfur.[16,17] Lu et al. devised a high-performance catalyst containing duple transition metal sulfides, in which the lattice stress and electron affinity of transition metal ions can regulate sulfides' electrochemical behaviors.[18] Similarly, Sun et al. synthesized single atom catalysts on double-shell nanocages for Li–S batteries. These single atom sites were occupied by transition metal atoms that triggered stepwise conversion reactions and improving their kinetics.[19] The transition metal compounds seemingly possess highly effective adsorption sites and exhibit significant catalytic potential, rendering them suitable for cathode modification in Li–S batteries.

The catalyst does not necessarily have strong adsorption properties, and vice versa. At present, however, it is rarely reported that two catalysts play the role of catalysis and adsorption respectively to achieve the modification of Li–S batteries. Therefore, exploring new interfacial chemistry that combines adsorption and catalytic conversion has been a research hotspot of Li–S batteries. Being extensively studied as catalyst materials for Li-S batteries, transition metal oxides, and transition metals often exhibit high catalytic or adsorptive properties, which can be attributed to the unique d-orbital structures. For instance, Pan et al. reported that finely dispersed Co clusters can significantly improve the diffusion kinetics of lithium, and enhanced the anchoring and reactivity of LiPSs on the cathode.[20] However, considering the high prices of transition metals like Co, two questions need to be answered: can we replace expensive transition metals with cheaper

H. Zhu, S. Chen, X. Yao, W. Zhao, T. Chen, L. Yang, F. Pan
School of Advanced Materials
Peking University
Shenzhen Graduate School
Shenzhen 518055, P. R. China
E-mail: yangly@pkusz.edu.cn; panfeng@pkusz.edu.cn
K. Yang
Advanced Technology Institute
Department of Electrical and Electronic Engineering
University of Surrey
Guildford, Surrey GU2 7XH, UK

The ORCID identification number(s) for the author(s) of this article can be found under https://doi.org/10.1002/adfm.202401470

DOI: 10.1002/adfm.202401470

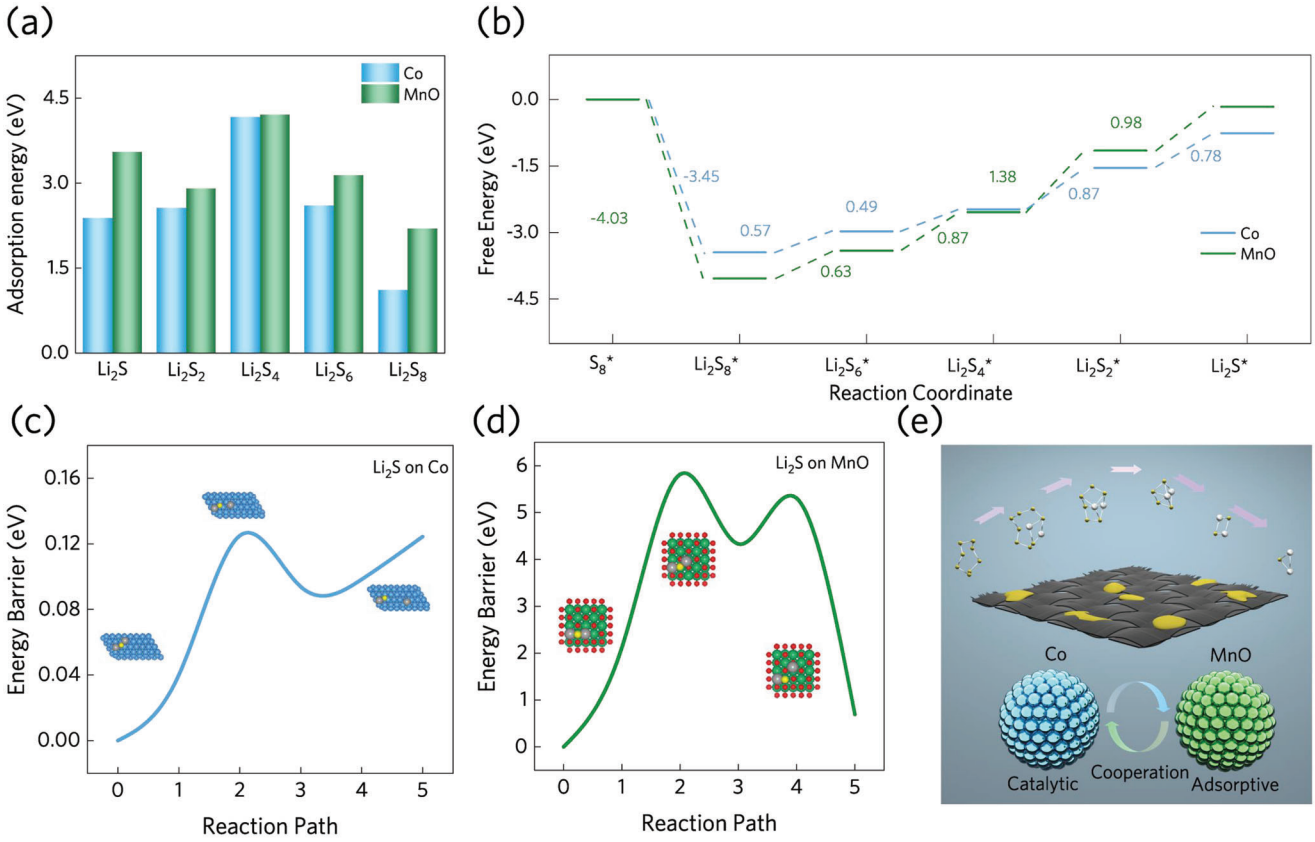

Figure 1. a) Binding energy of various sulfur species on Co or MnO catalytic surface; b) Gibbs free energy profiles for the multiphase sulfur conversion on Co or MnO catalytic surface; the decomposition energy profiles of Li_2S molecules on c) Co and d) MnO surfaces; e) Schematic of sulfur species conversion reaction.

ones and can we recycle these metals from waste materials for a second use?

2. Results and Discussion

2.1. Theoretical Prediction of Catalytic Property

In order to evaluate the chemisorption capacity and electrocatalytic effect of Co and MnO in Li–S batteries, the density functional theory (DFT) calculations were carried out. As shown in **Figure** 1a, the binding energies between polysulfides and the surface of Co/MnO were calculated (chemical models are presented in Figure S1, Supporting Information). An enhanced negative binding energy signifies a heightened capacity for chemical bonding, which is beneficial for homogenizing the LiPSs under lean electrolyte conditions.[21] Noticeably, the adsorption ability of MnO is stronger than Co, suggesting a better anchoring performance.

Additionally, the Gibbs free energy (ΔG) values of sulfur conversion process were calculated in Figure 1b. Generally, the liquid–solid conversion from Li_2S_4 to Li_2S_2 is regarded as the rate determining step (RDS) because of the sluggish kinetics. From the profile, Co presents the lower ΔG values (0.87 eV) for RDS than that of MnO (1.38 eV). Furthermore, the calculated ΔG for step ($Li_2S_2 \rightarrow Li_2S$) of MnO catalyst (0.98 eV) is higher than that of Co catalyst (0.78 eV), indicating that the formation Li_2S is thermodynamically favorable on Co active sites. On this basis, the energy barriers of Li_2S decomposition ($Li_2S \rightarrow LiS^- + Li^+$) on two substrates were calculated to evaluate the delithiation kinetics. As shown in Figure 1c,d, the decomposition energy of Li_2S on Co (0.12 eV) is much lower than that on MnO (2.16 eV). To sum up, Co catalyst could enhance the reaction kinetics of polysulfide and Mn catalyst strengthens the chemisorption with polysulfide (Figure 1e).

2.2. Synthesis and Characterization of Catalysts

As demonstrated in **Figure** 2a, the Co—MnO catalyst was fabricated from the spent $LiCoO_2$ (LCO) and $LiMn_2O_4$ (LMO) cathodes. The spent cathodes were collected from spent lithium-ion batteries (LIBs) and dissolved in nitric acid (the molar ratio of the two metals is 1:1) to obtain a mixed Co—Mn solution (Figure S4, Supporting Information). The carbon fiber (CF) was used to load the mixed salt and subsequently subjected to rapid thermal treatment under Ar-H_2 conditions, with a cut-off heating temperature of 1500 °C (denoted as Co—MnO@CF, more detailed synthesis information in the Experimental Section). The rapid thermal shock induces the formation of Co and MnO particles. The formation of manganese oxide is due to the lower first ionization

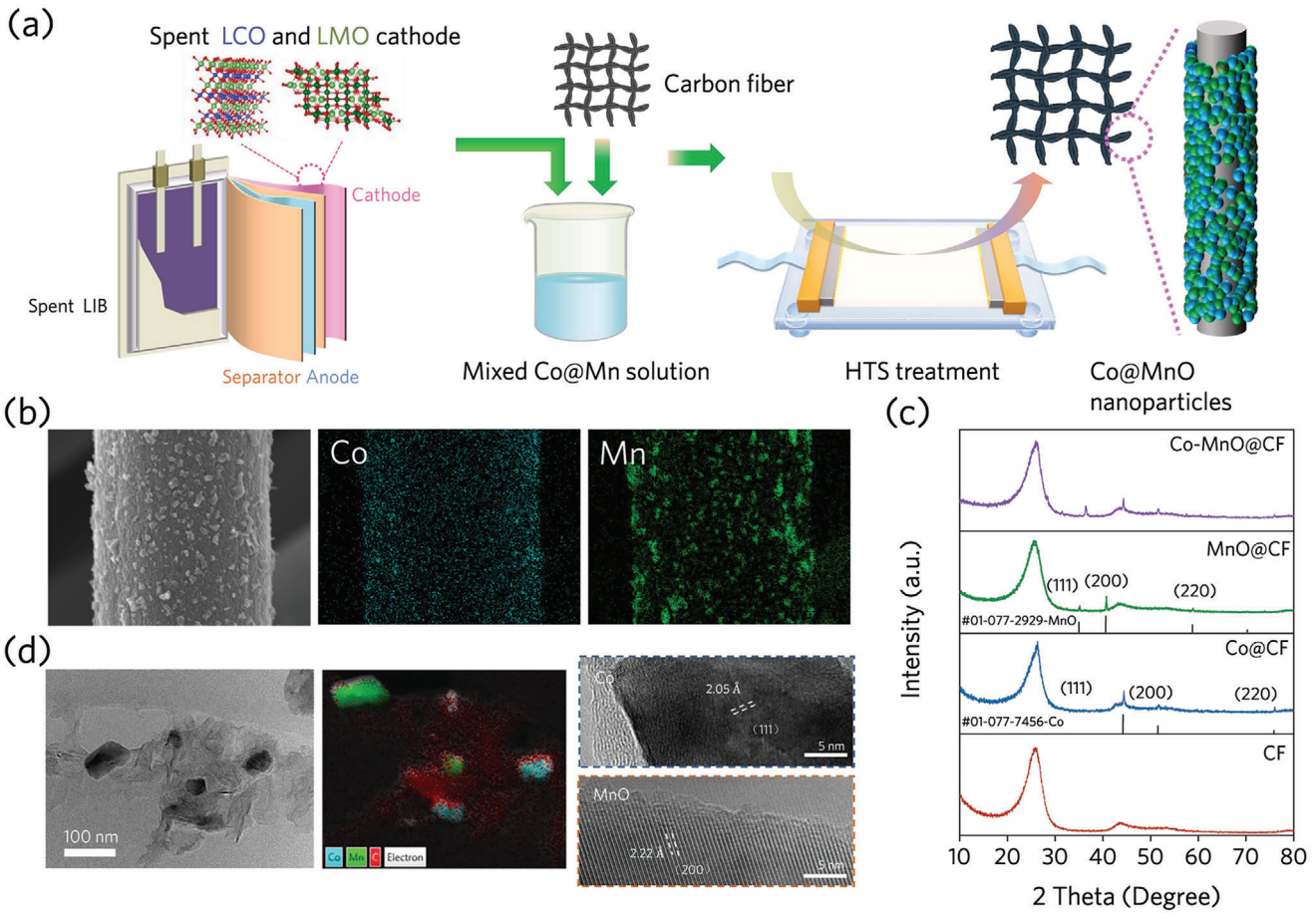

Figure 2. a) Schematic of the fabrication process of the Co—MnO catalyst from spent LIBs; b) SEM image and energy dispersive spectrometer mapping images of catalytic elements Co and Mn, scale bar = 2 μm; c) XRD pattern of various catalysts; d) HRTEM images of the Co—MnO catalyst.

energy of Mn (717 kJ mol^{-1}) compared with that of Co element (763 kJ mol^{-1}). For comparison, individual Co and MnO catalysts were also prepared using the same method.

As shown in Figure S6 (Supporting Information), the resulting areal mass loading of Co and MnO are measured to be 0.066 and 0.048 mg cm^{-2}, respectively, by inductively coupled plasma optical emission spectrometer (ICP-OES). After 2 s of HTS process, the Co and MnO particles were uniformly distributed on the CF (Figure 2b). By analyzing the element distribution of Co—MnO@CF, the particle size of MnO is larger than that of Co, which might be attributed to the higher melting point (1650 °C) of Mn compared with Co (1495 °C). More detailed scanning electron microscope (SEM) images of various catalyst@CF are presented in Figures S7–S9 (Supporting Information). The structural characteristics of various catalysts was investigated using the X-ray diffusion (XRD), as shown in Figure 2c. The broad peak at ≈26° could be ascribed to the existence of CF.[22] After undergoing the HTS process, the characteristic peaks of Co and MnO could be greatly identified according to the standard PDF cards (01-077-7456 and 01-077-2929), suggesting the formation of crystalline Co and MnO. The characteristic peak of Co at 778.3 eV and Mn^{2+} at 641.0 eV in the X-ray photoelectron spectra (XPS) also confirm the presence of Co and MnO (Figure S10, Supporting Information). Combined with the high-resolution TEM (HRTEM) images (Figure 2d; Figure S11, Supporting Information), the Co and MnO nanoparticles are dispersed on the CF, and the crystal structure in the particle center is confirmed to be Co (111) orientation and MnO (200) orientation. Although the distribution of Co varies with that of MnO, the DFT calculation results suggest as follows: during the S redox process, MnO sites absorb polysulfide species, serving as reservoirs for continuous reactions on adjacent Co sites. In addition, Raman peaks (Figure S12, Supporting Information) of Co-MnO@CF exhibits that the D and G peak intensity ratio (I_D/I_G) of CF decreased significantly after Co and MnO doping, suggesting the synergistic effect of improving the graphitization degree of the CF, hence the better conductivity.

2.3. Characterization of Reaction Kinetics

To investigate the electrocatalytic properties of different catalysts, a series of electrochemical tests were conducted for sulfur loaded carbon fiber (CF), Co@CF, MnO@CF, and Co—MnO@CF (denoted as S/CF, S/Co@CF, S/MnO@CF, and S/Co-MnO@CF, respectively). The cyclic voltammograms (CV) obtained from different cathodes (**Figure 3**a) exhibit two reduction peaks at 2.28 and 2.01 V, corresponding to the transition from S_8 to soluble long-chain LiPSs and further to Li_2S_2/Li_2S. The incorporation

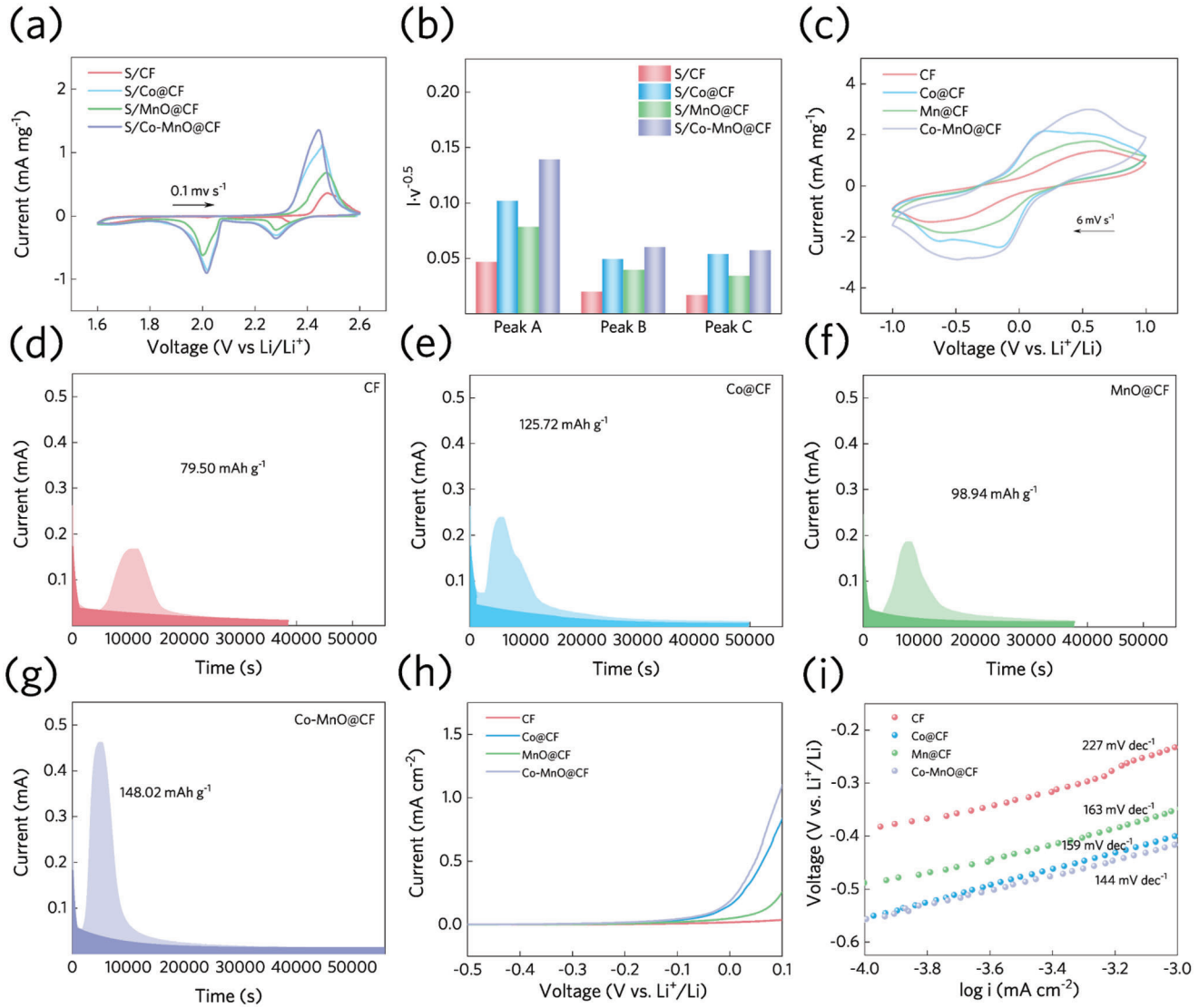

Figure 3. a) CV curves at 0.1 mV s^{-1} of the S/CF, S/Co@CF, S/MnO@CF, and S/Co-MnO@CF cathodes; b) $I \times \nu^{0.5}$ values at peak A, B, and C calculated from multi-rate CV curves of the S/CF, S/Co@CF, S/MnO@CF, and S/Co-MnO@CF cathodes; c) CV curves of Li_2S_6 symmetric cells with CF, Co@CF, MnO@CF, and Co-MnO@CF electrode; potentiostatic curves of Li_2S nucleation at 2.05 V on d) CF, e) Co@CF, f) Mn@CF, and g) Co-MnO@CF electrode; h) LSV plots and i) corresponding Tafel plots of Li_2S oxidation on four types of electrodes.

of a Co catalyst is beneficial for enhancing the reaction kinetics, and the S/Co—MnO@CF cathode exhibits an even higher peak current intensity, indicating exceptional sulfur utilization. Besides, multi-rate CV tests were used to explore the Li-ion diffusion rate under various electrodes (Figure S13, Supporting Information; Figure 3b).[23] According to the Randles–Sevcik law (as described in Supporting Information), the square root of sweep velocity ($\nu^{0.5}$) is linearly correlated with the peak current (I_p), and the Li-ion diffusion coefficient (D_{Li+}) could be obtained from the curve slope ($I_p/\nu^{0.5}$). D_{Li+} values of S/Co—MnO@CF cathode at peaks A, B, and C were calculated as 1.62×10^{-7}, 3.02×10^{-8}, and 2.74×10^{-8} cm^2 s^{-1}, respectively, higher than those of other cathodes (Figure S14, Supporting Information). Additionally, the S/Co—MnO@CF cathode exhibits distinct redox peaks and negligible overpotentials at high sweep rates, indicating its improved sulfur conversion kinetics. Simultaneously, the Li-ion diffusion rate of the S/Co@CF cathode surpasses that of the S/MnO@CF cathode, highlighting that Co catalysts are more conducive to enhancing Li-ion diffusion and accelerating reaction kinetics, which aligns with computational findings.

To elucidate the catalyzing efficacy of catalysts in the specific step of (poly)sulfide conversion, we first assembled symmetric cells utilizing Li_2S_6 as the active material. As depicted in Figure 3c, the current response of Co@CF surpassed that of MnO@CF, while Co—MnO@CF exhibited the highest response with the largest current plot area. These findings indicate superior catalytic capability of Co@CF compared to MnO, and a significantly enhanced reaction kinetics when both elements are simultaneously incorporated.[24] Additionally, the Li_2S precipitation tests for various electrodes were further conducted,

corresponding to the liquid–solid conversion from LiPSs to Li_2S.[25] As depicted in Figure 3d–g, the Li_2S deposition capacity was then determined by analyzing the current–time curves based on Faraday's law. Among the tested materials, Co—MnO@CF exhibited the highest Li_2S nucleation capacity (148.02 mAh g^{-1}), surpassing that of Co@CF (125.72 mAh g^{-1}) and MnO@CF (98.94 mAh g^{-1}). The capacity was directly calculated according to the peak area in light colors. The superior conversion capacity and faster nucleation response of Co—MnO@CF indicate that the incorporation of both Co and MnO can effectively reduce initial nucleation overpotential and accelerate the dynamic process of Li_2S formation. Furthermore, compared to the MnO@CF counterpart, the Co@CF electrode exhibits a larger and sharper nucleation peak, confirming that Co catalysts possess enhanced kinetics for LiPSs reduction compared to MnO catalysts.

Finally, linear sweep voltammetry (LSV) was used to study the oxidation behavior of Li_2S on different electrodes, as shown in Figure 3h. Compared with the pristine one, Co-MnO@CF greatly reduces the initial potential (from −0.416 to −0.581 V) and improves the current response. As shown in Figure 3i, the electrode containing Co—MnO@CF delivers the lowest Tafel gradient of 0.144 V dec^{-1}, indicating its capability of enhancing the electron migration ability and boosting the oxidation kinetics of Li_2S.[26,27] Similarly, Co@CF exhibits lower initial potential and Tafel gradient than MnO@CF, manifesting superior reaction kinetics.

2.4. Characterization of LiPSs Adsorption

As previously mentioned, Co exhibits superior catalytic properties compared to MnO in polysulfide conversion reactions, while the dual-component catalyst demonstrates the most effective enhancement of overall kinetics. Therefore, it is reasonable to speculate that the improved performance originates from a synergistic effect between Co and MnO, where MnO facilitates the adsorption of LiPSs. To validate our speculation, adsorption tests were conducted (Figure S15, Supporting Information) by immersing different hosts in a Li_2S_6 solution. After overnight stirring, the solution with bare CF remained yellow, while the solution with Co@CF collector still exhibited a yellowish hue. In stark contrast, the yellow Li_2S_6 solutions became clear and transparent when incorporating MnO catalysts into the electrode. This observation could be associated with the superior ability of MnO to adsorb LiPSs over Co. Hence, as expected, the adsorption performance of Co—MnO@CF lies between that of Co and MnO due to their equal proportions in this catalyst system. Additionally, offsite ultraviolet tests were performed on all four electrodes, where the temporal changes in intensity observed within the LiPS peak range (300–450 nm) are consistent with those manifested in optical images.[28]

To further investigate the adsorption behaviors, in situ Raman analysis was performed on the anode during galvanostatic cycling (**Figure 4**, measurement schematics in Figure S16, Supporting Information).[29] At open circuit voltage, no signals corresponding to active materials or LiPSs were detected in any cell. For the cell employing S/CF cathode, S_8^{2-} (215 cm^{-1}) and S_6^{2-} (399 cm^{-1}) peaks emerged in Raman spectra when discharged to the plateau at 2.3 V.[30,31] Then, S_4^{2-} (200 and 443 cm^{-1}) and dissociation products of S_6^{2-} (denoted by $-S_3^-$ at 533 cm^{-1}) appeared at the plateau of 2.1 V. The peak intensity and position of the LiPSs remain unchanged during the charging process from 1.6 to 2.6 V, indicating that bare CF suffers irreversible loss of active materials, ultimately leading to significant capacity decay of the cathode. For the cell with S/Co@CF cathode, weaker LiPS peaks arose during discharging and gradually diminished during charging. This result suggests that Co could alleviate the sulfide shuttle due to its adsorption ability.[29] As for S/MnO@CF, only weak S_6^{2-} and its dissociation product peaks emerged, which could be attributed to the strong adsorption tendency of LiPSs on MnO. Finally, despite the slightly weaker adsorbing capability, the S/Co—MnO@CF cell shows the similar behaviors as those of S/MnO@CF. Therefore, it can be speculated that in the presence of Co, LiPSs in the reaction may be rapidly converted into lithium sulfide, thus effectively reducing the formation and shuttle dose of LiPSs despite the amount of MnO in S/Co—MnO@CF is only half of that in S/MnO@CF. In a word, the combined effect of MnO and Co can enhance both catalytic and adsorptive properties of the cathode.

2.5. Electrochemical Performance of Co—MnO as Bifunctional Catalyst

Next, the electrocatalytic performance of various catalysts was evaluated by galvanostatic cycling tests. As displayed in **Figure 5a**, the S/Co—MnO@CF cathode delivered a higher initial capacity of 793 mAh g^{-1} at 1C than S/CF (615 mAh g^{-1}), S/Co@CF (725 mAh g^{-1}), and S/MnO@CF (691 mAh g^{-1}). Moreover, after 400 cycles, a capacity retention of 76.9% can be obtained by S/Co—MnO@CF, corresponding to a decay rate of 0.058% per cycle, which also significantly outperforms S/CF (0.18%), S/Co@CF (0.093%), and S/MnO@CF (0.12%). The capacity of the S/Co@CF cathode decreased steadily during cycling, suggesting the continuous loss of the reactants during the conversion reaction, which could be attributed to the weak LiPSs anchoring on Co. In comparison, the specific capacity of S/MnO@CF cathode decreased significantly during initial cycles and then stabilized after 200 cycles. It could be speculated that the sluggish reaction kinetics may have resulted in an excessive accumulation of long-chain LiPSs at the initial stage of the cycle, leading to saturation of active sites on MnO. Therefore, a portion of these LiPSs will inevitably shuttle to the anode, resulting in capacity loss. After the excess LiPSs are consumed, the remaining LiPSs can be reversibly converted on MnO@CF. The above speculation is verified by the XPS results of lithium anode after cycling (Figure S17, Supporting Information), where the peak intensity variation of Li_2S_x ($x \leq 4$) and Li_2S_x ($x > 4$) for the cell using S/Co@CF and S/MnO@CF showed different tendencies. The amount of LiPSs in was steadily increasing in S/Co@CF during the cycling process, while that of the S/MnO@CF group was relatively high at the 100th cycle but remained at the same level after the 400th cycle.[32,33] From these findings, it can be concluded that under a relatively high concentration of LiPSs, the electrochemical reaction kinetics determine the shuttling phenomena; whereas under a lower polysulfides concentration, the confining strength of the substrate become the main factor. Consequently,

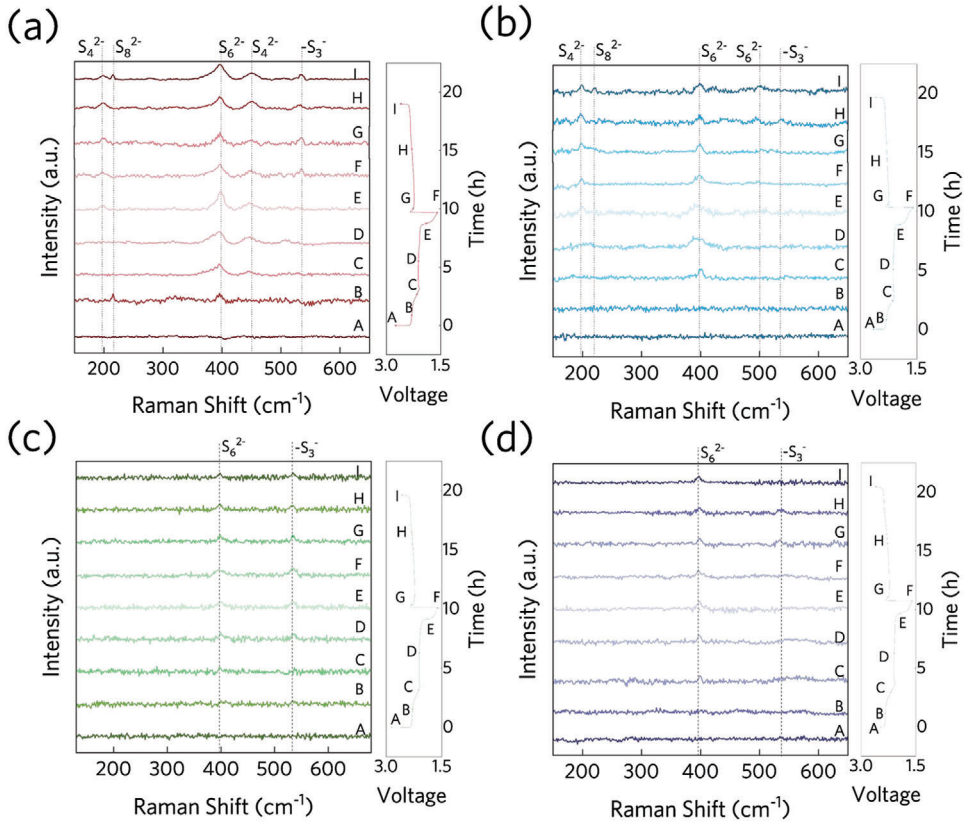

Figure 4. In situ Raman spectra of Li-S batteries with a) S/CF, b) S/Co@CF, c) S/MnO@CF and, d) S/Co-MnO@CF cathodes during a galvanostatic process at the current density of 0.2C.

the co-doping of Co and MnO inhibits shuttle effects while promoting electrochemical conversion kinetics.

To obtain more information about the conversion reaction of active substances in positive electrochemical process, the specific capacity–voltage distribution diagram of galvanostatic charge–discharge process (Figure 5b) was studied. The overpotential (ΔV) of the S/Co—MnO@CF cathode during the charging and discharging period was the lowest (146 mV), manifesting its superior kinetics. Moreover, the discharge interval could be further subdivided, and the discharge capacity of each cathode was quantitatively evaluated noted by C_H [discharge capacity from open-circuit voltage to the start of the last discharge plateau (≈2.06 V)] and C_L (the remaining discharge capacity).[34] The higher proportion of the lower platform indicated that more soluble LiPSs participated in the reaction and lower loss occurred. The C_L/C_H value of the S/Co-MnO@CF cathode is 2.20, higher than that of S/Co@CF (1.90), S/MnO@CF (2.10,) and S/CF (1.644) cathode. These results indicate that MnO-containing catalysts can more effectively confine the intermediate products of active substances to the cathodic region. The electrochemical impedance spectra (EIS) of the four cathodes after 100 cycles (Figure 5c) show that the S/Co—MnO@CF cathode has the smallest R_{ct} and the largest slope, indicating that Co and MnO jointly accelerate the transfer of charge on the electrode surface and promote the ion diffusion process. The in situ impedance spectra of different cells (Figure S18, Supporting Information) exhibit similar phenomena.

The rate performance of cathodes was further evaluated at different C-rates from 0.5C to 4C (Figure 5d). The cell with S/Co—MnO@CF exhibits higher specific capacities (904, 821, 764, and 707 mAh g^{-1} at 0.5C, 1C, 2C, and 4C, respectively) than the other three cells across all C-rates. The high electrocatalytic capability and LiPS adsorption capacity of Co—MnO synergistically accelerates the LiPSs conversion reaction at high rates, effectively anchoring LiPSs and reducing the overpotential of the cell (Figure S19, Supporting Information). Furthermore, a comparison with recent literature (shown in Figure 5e) reveals that the rate performance of S/Co—MnO@CF cathode surpasses materials with similar transition metals or catalysts. The advantages of S/Co—MnO@CF in both cycling stability and rate capability indicate that the proposed cathode design and synthesis strategy has great potentials to cope with various working conditions.

For commercial Li–S batteries, the sulfur loading density is also a crucial parameter.[35,36] Typically, lab-prepared Li–S batteries have low areal loads and high electrolyte/sulfur ratios (E/S, μL mg^{-1}), that fall far short of commercially required energy densities. Therefore, S/Co—MnO@CF cathodes with higher areal loadings (5.6 mg cm^{-2}) were prepared, with a controlled E/S ratio of 8. As shown in Figure 5f, it demonstrated high initial specific areal capacity of 4.98 mAh cm^{-2} at 0.2C, respectively. After 100 cycles, capacity retentions can be achieved for 70.0%, respectively, which corresponding to fading rates of 0.3% per cycle. To further demonstrate the potentials of

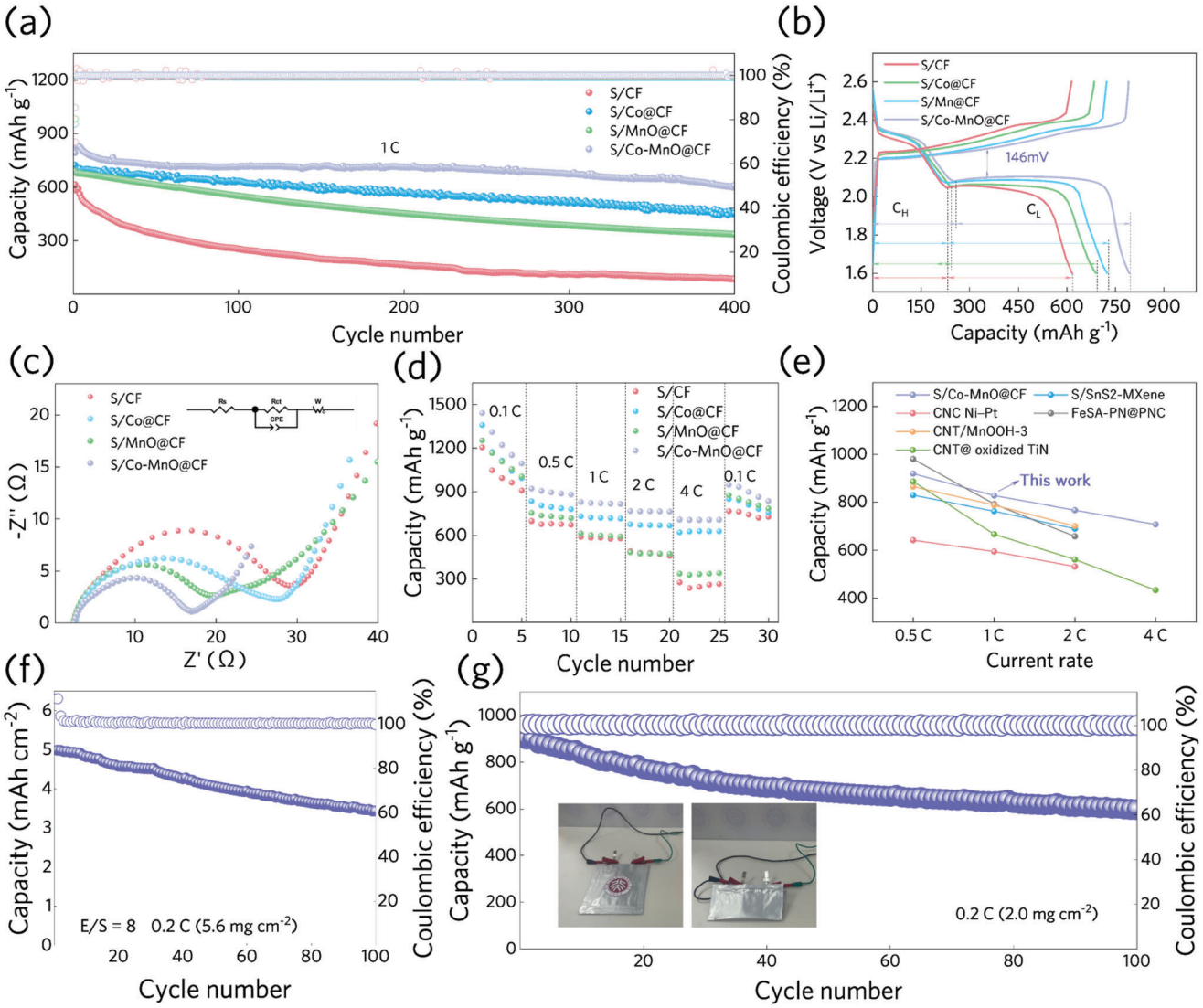

Figure 5. Electrochemical performance of the S/CF, S/Co@CF, S/MnO@CF, and S/Co-MnO@CF cathodes. a) Cycling performance at 1C. b) The comparison galvanostatic charge/discharge curves for the 1st cycle. c) EIS spectra after 100 cycles at 1C. d) The comparison of rate performance. e) The discharge capacity of S/Co—MnO@CF cathode compared with other similar materials reported at different current rates. The complete original data are shown in Table S1 (Supporting Information). f) Cycling performance of S/Co—MnO@CF cathode under high sulfur loading of 5.6 mg cm^{-2} at 0.2C. g) Cycling performance of the S/Co—MnO@CF pouch cell after being bent 180° under sulfur loading of 2.0 mg cm^{-2} at 0.2C.

S/Co—MnO@CF in practical use, proof-of-concept pouch cells were assembled with ≈200 µm thick lithium anode and tested (Figure 5g; Figure S20, Supporting Information). The flexible Li–S pouch cell based on S/Co—MnO@CF delivers an initial discharge capacity of 899 mAh g^{-1} and a capacity retention of 67.4% after 100 cycles at 0.2C when being bent 180°. Additionally, we conducted an assessment of the energy consumption associated with the HTS technology and performed an economic analysis on the viability of transition metals in the electrodes.[37,38] The final findings elucidate that the upcycling strategy exhibits reduced energy consumption, while simultaneously achieving a higher utilization rate of transition metals in the obtained electrodes.[39] All these results demonstrate the great application potential of S/Co—MnO@CF cathode in the future portable electronics.

3. Conclusion

In summary, we developed a high-temperature shock method to convert spent cathodes in LIBs into Co—MnO catalysts for Li–S batteries. Ex situ and in situ characterizations have confirmed that Co catalyst contributes to reducing the Li^+ diffusion barrier enabling to enhance the reaction kinetics of LiPSs and MnO catalyst provides the strong anchoring site with LiPSs, enhancing molecular anchoring interaction. As a result, the S/Co—MnO@CF cathode exhibits an excellent cycling stability with a low-capacity decay rate of 0.058% per cycle over 400 cycles at 1C, and outstanding rate capability. Under a sulfur loading of 5.6 mg cm^{-2}, stable cycling performance of an area capacity of 3.46 mAh cm^{-2} for 100 cycles is achieved, demonstrating its potential in high-energy Li–S batteries. The proposed

strategy provides a new direction for the design of Li–S battery catalysts and paves an effective way to reuse spent cathodes such as Ni—Co—Mn tertiary materials.

Supporting Information

Supporting Information is available from the Wiley Online Library or from the author.

Acknowledgements

F.P. acknowledge the support from Shenzhen Science and Technology Research Grant (ZDSYS201707281026184). F.P. acknowledge the support from Soft Science Research Project of Guangdong Province (2017B03031013). L.Y. acknowledge the support from Shenzhen Science and Technology Planning Project (JSGG20220831095604008).

Conflict of Interest

The authors declare no conflict of interest.

Data Availability Statement

Research data are not shared.

Keywords

catalysis, cathode upcycling, high-temperature shock, lithium–sulfur battery

Received: January 24, 2024
Revised: March 29, 2024
Published online: April 13, 2024

[1] J. B. Goodenough, K.-S. Park, *J. Am. Chem. Soc.* **2013**, *135*, 1167.
[2] J. B. Goodenough, *Acc. Chem. Res.* **2013**, *46*, 1053.
[3] X. Ji, K. T. Lee, L. F. Nazar, *Nat. Mater.* **2009**, *8*, 500.
[4] L. Zhou, D. L. Danilov, F. Qiao, J. Wang, H. Li, R.-A. Eichel, P. H. L. Notten, *Adv. Energy Mater.* **2022**, *12*, 2202094.
[5] H. Li, H. Yang, X. Ai, *Adv. Mater.* **2024**, 2305038.
[6] R. Fang, S. Zhao, Z. Sun, D.-W. Wang, H.-M. Cheng, F. Li, *Adv. Mater.* **2017**, *29*, 1606823.
[7] A. Rosenman, E. Markevich, G. Salitra, D. Aurbach, A. Garsuch, F. F. Chesneau, *Adv. Energy Mater.* **2015**, *5*, 1500212.
[8] H.-J. Peng, J.-Q. Huang, X.-B. Cheng, Q. Zhang, *Adv. Energy Mater.* **2017**, *7*, 1700260.
[9] A. Kim, S. H. Oh, A. Adhikari, B. R. Sathe, S. Kumar, R. Patel, *J. Mater. Chem. A* **2023**, *11*, 7833.
[10] Y. Liu, Y. Elias, J. Meng, D. Aurbach, R. Zou, D. Xia, Q. Pang, *Joule* **2021**, *5*, 2323.
[11] C.-X. Bi, L.-P. Hou, Z. Li, M. Zhao, X.-Q. Zhang, B.-Q. Li, Q. Zhang, J.-Q. Huang, *Energy Mater. Adv.* **2024**, *4*, 0010.
[12] M. Zhang, W. Chen, L. Xue, Y. Jiao, T. Lei, J. Chu, J. Huang, C. Gong, C. Yan, Y. Yan, Y. Hu, X. Wang, J. Xiong, *Adv. Energy Mater.* **2020**, *10*, 1903008.
[13] B.-J. Lee, C. Zhao, J.-H. Yu, T.-H. Kang, H.-Y. Park, J. Kang, Y. Jung, X. Liu, T. Li, W. Xu, X.-B. Zuo, G.-L. Xu, K. Amine, J.-S. Yu, *Nat. Commun.* **2022**, *13*, 4629.
[14] Y. Guo, R. Khatoon, J. Lu, Q. He, X. Gao, X. Yang, X. Hu, Y. Wu, J. Lian, Z. Li, Z. Ye, *Carbon Energy* **2021**, *3*, 841.
[15] H. Xu, R. Hu, Y. Zhang, H. Yan, Q. Zhu, J. Shang, S. Yang, B. Li, *Energy Storage Mater.* **2021**, *43*, 212.
[16] T. Wang, J. He, Z. Zhu, X.-B. Cheng, J. Zhu, B. Lu, Y. Wu, *Adv. Mater.* **2023**, *35*, 2303520.
[17] J. Qin, R. Wang, P. Xiao, D. Wang, *Adv. Energy Mater.* **2023**, *13*, 2300611.
[18] Z. Shen, X. Jin, J. Tian, M. Li, Y. Yuan, S. Zhang, S. Fang, X. Fan, W. Xu, H. Lu, J. Lu, H. Zhang, *Nat. Catal.* **2022**, *5*, 555.
[19] L. Ren, K. Sun, Y. Wang, A. Kumar, J. Liu, X. Lu, Y. Zhao, Q. Zhu, W. Liu, H. Xu, X. Sun, *Adv. Mater.* **2023**, *36*, 2310547.
[20] R. Wang, J. Yang, X. Chen, Y. Zhao, W. Zhao, G. Qian, S. Li, Y. Xiao, H. Chen, Y. Ye, G. Zhou, F. Pan, *Adv. Energy Mater.* **2020**, *10*, 1903550.
[21] Z. Yu, X. Huang, M. Zheng, S.-Q. Zhang, Y. Yang, J. Lu, *Adv. Mater.* **2023**, *35*, 2300861.
[22] C.-C. Lai, C.-T. Lo, *Electrochim. Acta* **2015**, *183*, 85.
[23] Y. Wang, R. Zhang, J. Chen, H. Wu, S. Lu, K. Wang, H. Li, C. J. Harris, K. Xi, R. V. Kumar, S. Ding, *Adv. Energy Mater.* **2019**, *9*, 1900953.
[24] X. Zhang, T. Yang, Y. Zhang, X. Wang, J. Wang, Y. Li, A. Yu, X. Wang, Z. Chen, *Adv. Mater.* **2023**, *35*, 2208470.
[25] F. Y. Fan, W. C. Carter, Y. M. Chiang, *Adv. Mater.* **2015**, *27*, 5203.
[26] Y. Zhang, J. Liu, J. Wang, Y. Zhao, D. Luo, A. Yu, X. Wang, Z. Chen, *Angew. Chem.–Int. Ed.* **2021**, *60*, 26622.
[27] Q. Zhang, W. Shen, P. Li, J. Song, L. Zhu, E. Han, R. Wang, X. Li, *Chin. J. Struct. Chem.* **2023**, *42*, 100134.
[28] D. Zhang, S. Wang, R. Hu, J. Gu, Y. Cui, B. Li, W. Chen, C. Liu, J. Shang, S. Yang, *Adv. Funct. Mater.* **2020**, *30*, 2002471.
[29] L. Xue, Y. Li, A. Hu, M. Zhou, W. Chen, T. Lei, Y. Yan, J. Huang, C. Yang, X. Wang, Y. Hu, J. Xiong, *Small Struct* **2022**, *3*, 2100170.
[30] M. Hagen, P. Schiffels, M. Hammer, S. Dörfler, J. Tübke, M. J. Hoffmann, H. Althues, S. Kaskel, *J. Electrochem. Soc.* **2013**, *160*, A1205.
[31] J. J. Chen, R. M. Yuan, J. M. Feng, Q. Zhang, J. X. Huang, G. Fu, M. Sen Zheng, B. Ren, Q. F. Dong, *Chem. Mater.* **2015**, *27*, 2048.
[32] Y. Diao, K. Xie, S. Xiong, X. Hong, *J. Electrochem. Soc.* **2012**, *159*, A1816.
[33] M. I. Nandasiri, L. E. Camacho-Forero, A. M. Schwarz, V. Shutthanandan, S. Thevuthasan, P. B. Balbuena, K. T. Mueller, V. Murugesan, *Chem. Mater.* **2017**, *29*, 4728.
[34] Y. Tsao, M. Lee, E. C. Miller, G. Gao, J. Park, S. Chen, T. Katsumata, H. Tran, L. W. Wang, M. F. Toney, Y. Cui, Z. Bao, *Joule* **2019**, *3*, 872.
[35] J. Wang, X. Yan, Z. Zhang, H. Ying, R. Guo, W. Yang, W.-Q. Han, *Adv. Funct. Mater.* **2019**, *29*, 1904819.
[36] M. Rana, S. A. Ahad, M. Li, B. Luo, L. Wang, I. Gentle, R. Knibbe, *Energy Storage Mater.* **2019**, *18*, 289.
[37] L. Reinhart, D. Vrucak, R. Woeste, H. Lucas, E. Rombach, B. Friedrich, P. Letmathe, *J Clean Prod* **2023**, *416*, 137834.
[38] E. A. Othman, A. G. J. van der Ham, H. Miedema, S. R. A. Kersten, *Sep. Purif. Technol.* **2020**, *252*, 117435.
[39] S. Xiong, J. Ji, X. Ma, *Waste Manage.* **2020**, *102*, 579.